YU.V. KLYSKO, S.V. SYROTYUK

Semiconductor Electronics Department, Lviv Polytechnic National University
*(12, S. Bandera Str., Lviv 79013, Ukraine; e-mail: yuraklisko@gmail.com)*

# HYBRID FUNCTIONAL ANALYSIS OF ELECTRONIC PROPERTIES OF TRANSITION-METAL PHTHALOCYANINES

UDC 538

*This work presents the ab initio study of transition-metal phthalocyanines within a PBE0 hybrid functional. The list of metal impurities includes manganese, iron, cobalt, nickel, copper, and zinc. All calculations of isolated molecules have been performed with the use of the projector augment-wave method. For iron phthalocyanine, we have performed four calculations with different values of the mixing parameter $\alpha$ (the value of the exact exchange) – 0, 1/4, 1/3, and 1/2. For all other molecules, the calculations have been performed for $\alpha = 1/4$ and 1/3. The electronic structure parameters including the HOMO-LUMO energy gap, Fermi level, magnetization, and imaginary part of the dielectric function are presented and compared with available theoretical and experimental data. Manganese, iron, and cobalt phthalocyanines show a strong dependence of electronic properties on the value of the exact exchange interaction. In other molecules with nickel, copper, and zinc, this dependence is not significant.*

*K e y w o r d s*: organometallic materials, hybrid functionals.

## 1. Introduction

Metal phthalocyanine complexes is a group of metal-organic materials. Each complex is a planar molecule of phthalocyanine with a metal atom inside the inner C–N ring including 18 $\pi$-electrons. Metal-phthalocyanines are widely investigated for electronics purposes and for organic photovoltaics especially. Some phthalocyanines are already well-known dyes. It is worth to note that, during the last decades, organic dyes were intensively studied for electronics purposes. The cause is in the processability and/or some unique characteristics of some agents. In addition to perylene-based dyes which are to be small molecule acceptors in organic photovoltaics (OPV) heterostructures, phthalocyanines are explored as small molecule donor materials [1–5] and organic-inorganic interfaces [6–9]. Phthalocyanines are also attractive for OPV due the possibility to convert light into electricity in the near-infrared (NIR) region [10–12].

Beside the light conversation and light emitting devices [13–15] including the photodynamic therapy [16, 17], phthalocyanine are widely studied in the field of organic field transistors [18], gas sensors [19], and biosensors [20, 21].

In the case of transition-metal phthalocyanines, researchers explore the behavior of *d*-electrons and the interaction with different substrates (graphene, gold, *etc.*) in order to get the possibility to use these materials in spintronics [22–26].

This work is supposed to consider the electronic properties of a number of transition-metal-phthalocyanines (Fig. 1) within a PBE0 hybrid functional and to analyze the impact of the exact exchange and self-interaction of *d*-electrons in metal-organic systems.

© YU.V. KLYSKO, S.V. SYROTYUK, 2021

## 2. Methods

The hybrid functional is a mixing of an implicit exact-correlation potential with the exact Hartree–Fock (exchange) potential. This trick is supposed to solve the band-gap problem in density functional theory (DFT). Both local (LDA) and semilocal (GGA) approximations of DFT underestimate the value of the electron energy gap in solids, as well as in molecules or other bounded systems [27–29]. As the cause for this fact, we consider the self-interaction which is canceled in the Hartree–Fock theory. The influence of the self-interaction rises with the orbital angular momentum. The reduction of the self-interaction for $d$-states is essential in order to obtain accurate results. Here, we are going to use a PBE0 functional in order to describe metal-organic complexes by the example of metal-phthalocyanines.

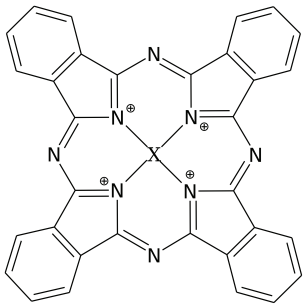


X = Mn, Fe, Co, Ni, Cu, Zn

***Fig. 1.*** Chemical structure of the phthalocyanines under study

*Table 1.* **The initial options for the PAW generation: the cut-off radii $r_c$ and valence basis states**

| Atom | $r_c, r_{\text{Bohr}}$ | Valence states |
|---|---|---|
| H | 0.9 | $1s^1$ |
| C | 1.3 | $2s^2 2p^2$ |
| Mn | 2.1 | $3s^2 3p^6 3d^6 4s^1$ |
| Fe | 2.1 | $3s^2 3p^6 3d^7 4s^1$ |
| Co | 2.1 | $3s^2 3p^6 3d^8 4s^1$ |
| Ni | 1.8 | $3s^2 3p^6 3d^8 4s^2$ |
| Cu | 2.0 | $3s^2 3p^6 3d^{10} 4s^1$ |
| Zn | 2.3 | $3d^{10} 4s^2$ |

*Table 2.* **PBE0 electronic structure parameters of FePc obtained with four different mixing parameters $\alpha$**

| $\alpha$ | $E_g$, eV | $E_f$, eV | $m$, $\mu_B$ |
|---|---|---|---|
| 0 | 1.45/0.06 | –1.68 | 2.05 |
| 1/4 | 1.43/1.31 | –1.71 | 2.00 |
| 1/3 | 1.38/0.91 | –1.52 | 2.29 |
| 1/2 | 1.37/0.96 | –1.48 | 4.35 |

The general formula describing the PBE0 formalism is as follows:

$$E_{xc}^{\text{PBE0}} = \alpha E_x^{\text{HF}} + (1-\alpha) E_x^{\text{PBE}} + E_c^{\text{PBE}}, \tag{1}$$

where $E_{xc}^{\text{PBE0}}$ is the hybrid PBE0 exchange-correlation potential, $E_x^{\text{HF}}$ is the exact Hartree–Fock exchange, and $E_x^{\text{PBE}}$ and $E_c^{\text{PBE}}$ are the approximated exchange and correlation potentials proposed in [30]. The coefficient $\alpha$ determines the value of the exact exchange.

We have carried out calculations of the ground state within the Projector Augmented Wave (PAW) method [31]. This method combines pseudopotentials with the linearized augmented plane waves (LAPW) method. In this case, we can get an auxiliary wave function $\tilde{\psi}_n$ from the exact all-electron Kohn–Sham wave function $\psi_n$, using the transformation operator as follows:

$$|\psi_n\rangle = \hat{T}|\tilde{\psi}_n\rangle, \tag{2}$$

where index $n$ includes **k** index, band index, and spin index. This expression results in a new form of the Kohn–Sham equation:

$$\hat{T}^\dagger \hat{H} \hat{T} |\tilde{\psi}_n\rangle = \epsilon_n \hat{T}^\dagger \hat{T} |\tilde{\psi}_n\rangle. \tag{3}$$

The transformation operator $\hat{T}$ can be atom-centered transformed into the following form:

$$\hat{T} = 1 + \sum_a \hat{T^a} = 1 + \sum_a \sum_i (|\phi_i^a\rangle - |\tilde{\phi}_i^a\rangle)\langle \tilde{p}_i^a|, \tag{4}$$

where $\hat{T^a}$ is non-zero only inside a sphere centered at an atom $a$ with a radius $r_c$. The quantities $\phi_i^a$ and $\tilde{\phi}_i^a$ present the true and smooth partial waves, respectively, and $\tilde{p}_i^a$ is the smooth projector satisfying the relation

$$\langle \tilde{p}_i^a | \tilde{\phi}_j^a \rangle = \delta_{i,j}, \quad r < r_c^a. \tag{5}$$

The summary of PAW options is presented in Table 1. All calculations have been performed, by using the ABINIT code [32]. Molecular geometries have been optimized by a simple relaxation of the ionic

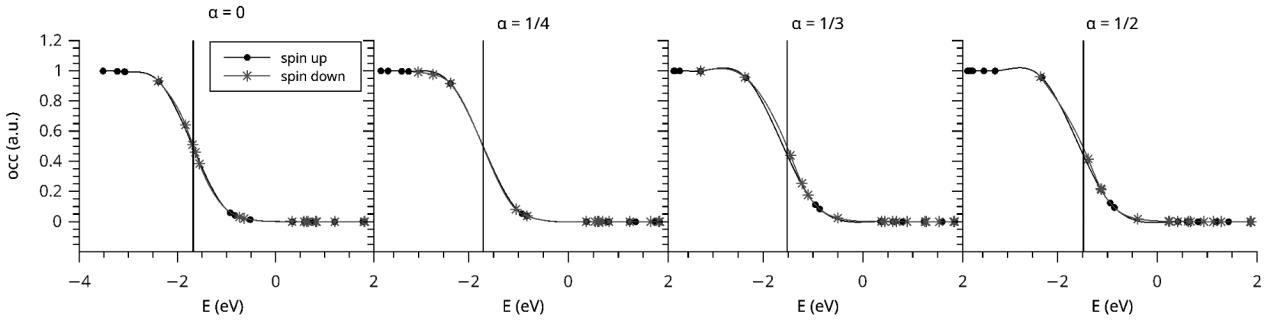


***Fig. 2.*** Occupation of spin-polarized electrons zin FePc obtained with different mixing parameters $\alpha$. Drop black line represents the Fermi level

*Table 3.* **PBE0 electronic structure parameters of transition-metal phthalocyanines obtained with two mixing parameters, $\alpha$. The column "other" contains the information about other *ab initio* studies with several hybrid functionals (noted in scopes) and experimental data on the magnetic state**

| | PBE0 ($\alpha = 1/4$) | | | PBE0 ($\alpha = 1/3$) | | | Other | |
|---|---|---|---|---|---|---|---|---|
| | $E_g$, eV | $E_f$, eV | $E_g$, eV | $m, \mu_B$ | $E_f$, eV | $m$, $\mu_B$ | $E_g$, eV | Spin |
| MnPc | 1.38/1.04 | –1.42 | 3.41 | 1.37/1.07 | –1.40 | 3.45 | 0.9 (HSE06) [33]<br>1.4 (B3LYP) [33]<br>0.4 (DFT + U, U = 5 eV) [33]<br>1.4 (PBE0) [37]<br>1.4 (HSE) [37] | 3/2 [34–36] |
| FePc | 1.43/1.31 | –1.71 | 2.00 | 1.38/0.91 | –1.52 | 2.29 | 1.38 (VNW+UHF) [38]<br>1.5 (HSE06) [33]<br>1.9 (B3LYP) [33]<br>1.3 (DFT + U, U = 5 eV) [33]<br>1.8 (B3LYP) [41] | 1 [39, 40] |
| CoPc | 1.39/0.08 | –1.61 | 1.09 | 1.41/1.30 | –1.64 | 2.91 | 1.96 (VNW+UHF) [38]<br>1.8 (HSE06) [33]<br>2.2 (B3LYP) [33]<br>1.5 (DFT + U, U = 5 eV) [33] | 1/2 [36, 42, 43] |
| NiPc | 1.41/1.41 | –1.72 | 0.00 | 1.41/1.41 | –1.72 | 0.00 | 1.47 (VNW+UHF) [38]<br>1.8 (HSE06) [33]<br>2.2 (B3LYP) [33]<br>1.5 (DFT + U, U = 5 eV) [33] | 0 [42] |
| CuPc | 0.76/0.76 | –1.63 | 0.00 | 0.82/0.82 | –1.59 | 0.00 | 1.42 (VNW+UHF) [38]<br>1.8 (HSE06) [33]<br>2.2 (B3LYP) [33]<br>1.4 (DFT + U, U = 5 eV) [33]<br>2.3 (PBE0) [44] | 1/2 [35, 36] |
| ZnPc | 1.35/1.35 | –1.63 | 0.00 | 1.35/1.35 | –1.64 | 0.00 | 1.91 (VNW+UHF) [38]<br>2.2 (B3LYP) [41]<br>2.0 (B3LYP) [45] | |

positions according to the force convergence. Having performed the convergence study, we have defined the optimal plane wave cutoff energies: 30 Ha for the wave function, 140 Ha for the electron density and potentials, and 3 Ha for RPA dielectric matrix. All molecules have been calculated, by using the set consisting of 190 bands with metallic occupation described by the Fermi–Dirac smearing.

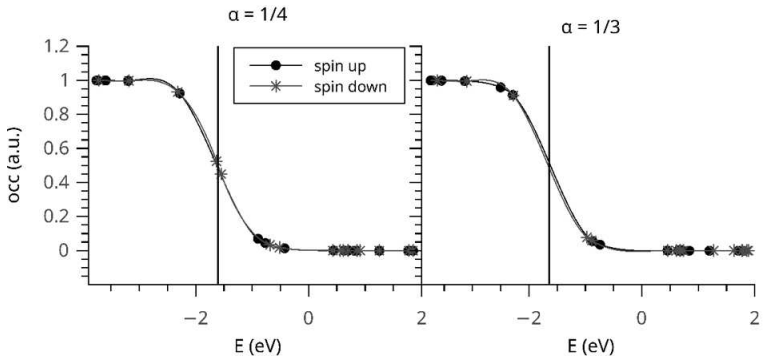


***Fig. 3.*** Occupation of spin-polarized electrons in CoPc obtained within different mixing parameters $\alpha$. Drop black line represents the Fermi level

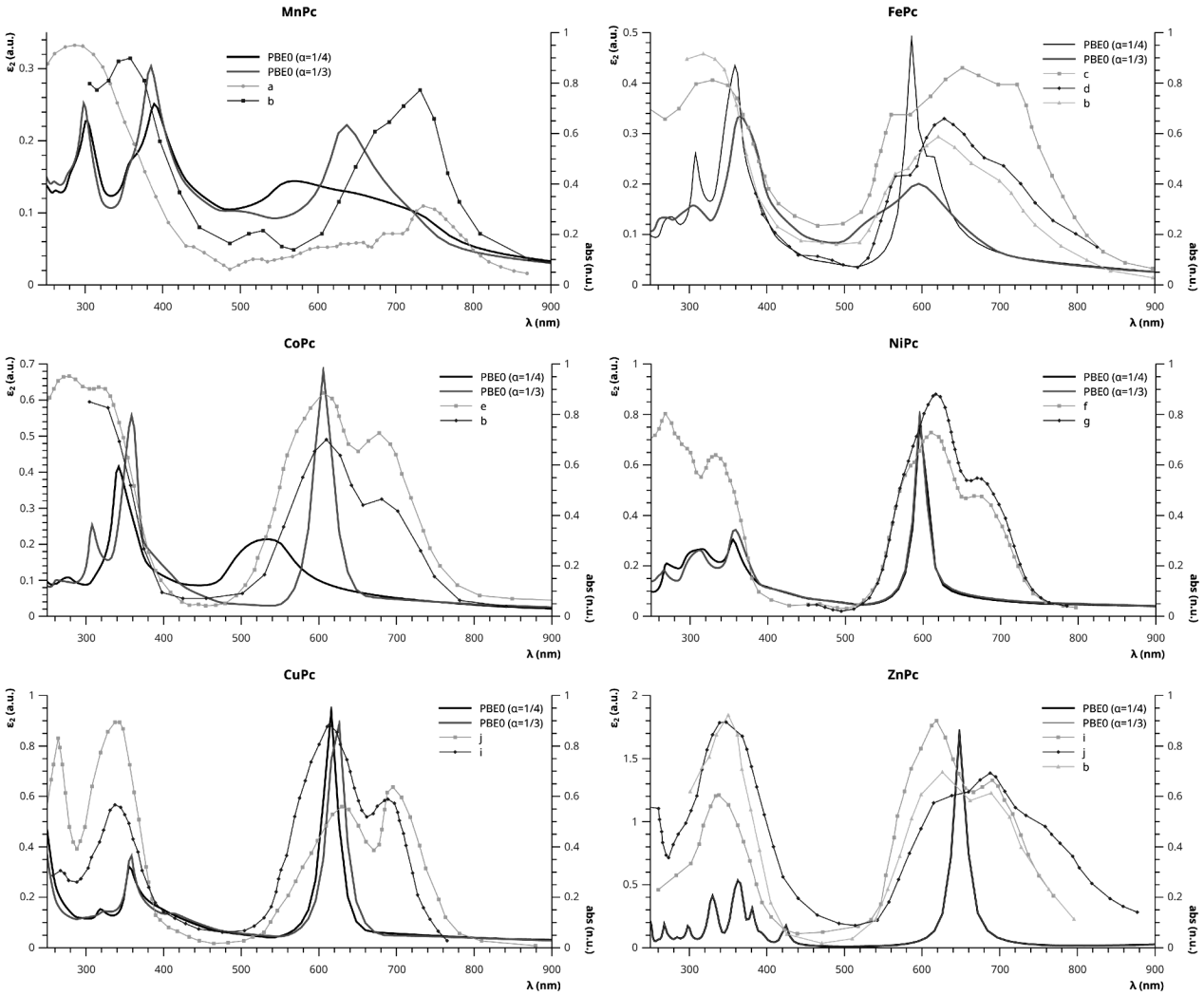


***Fig. 4.*** Imaginary part of DF obtained in RPA on the base of PBE0 with $\alpha = 1/4$ and $1/3$ in comparison with experimental absorption spectra. *a* – [46], *b* – [47], *c* – [48], *d* – [49], *e* – [50], *f* – [51], *g* – [52], *h* – [53], *i* – [54], *j* – [55]

## 3. Results and Discussion

For iron (II) phthalocyanine (FePc), we have performed four calculations with different mixing factors: the pure PBE with $\alpha = 0$, and the hybrid ones with $\alpha = 1/4$, $1/3$, and $1/2$. The main results for FePc are presented in Table 2. We can admit a slight dependence of the energy band gap $E_g$ for a spin-up electron. Meanwhile, a significant diversity of $E_g$ is observed in the case of a spin-down one. Spin-polarized electron occupations are presented in Fig. 2. In the case of a non-hybrid functional ($\alpha = 0$), we can observe a smearing of spin-down electrons around the Fermi level $E_f$ caused by using the Fermi–Dirac distribution. In the case of $\alpha = 1/4$, we observe a slight difference between spin-up and spin-down electron levels with the Fermi level $E_f$ close to the middle of $E_g$. In the cases where $\alpha = 1/3$ and $1/2$, the electronic parameters ($E_g$ and $E_f$) and occupations are quite similar, but the magnetization $m$ is almost twice higher (Table 2).

We have performed PBE0 calculations for the list of materials (Fig. 1) with $\alpha = 1/4$ and $1/3$ (Table 3). We also have obtained the frequency-dependent dielectric function (DF) in the Random Phase Approximation (RPA). The imaginary part of DF $\epsilon_2$ is presented in Fig. 4.

Considering MnPc, we can note a slight dependence of both electronic ($E_g$ and $E_f$) and magnetic ($m$) properties on the parameter $\alpha$ (Table 3). MePc has magnetization $m$ around 3.4 $\mu_B$.

Similarly to FePc, a strong impact of the mixing factor $\alpha$ have been found in CoPc with a smeared spin-down electron is observed in CoPc with $\alpha = = 1/4$ (Fig. 3). In addition to the difference in electronic parameters, we have noticed a high difference in magnetic properties: the total magnetization in CoPc with $\alpha = 1/3$ is almost three times higher than in in CoPc with $\alpha = 1/4$. Comparing $\epsilon_2$ with experimental absorption spectra in CoPc, we can say that PBE0 ($\alpha = 1/3$) shows a better agreement.

## 4. Conclusions

The values of $1/4$ and $1/3$ of the coefficient $\alpha$ formally mean a smaller and larger admixture of the exact Hartree–Fock exchange in the exchange-correlation functional. It is worth analyzing how the choice of the exchange-correlation functional influences the results of calculations of the dielectric function shown in Fig. 4. From Fig. 4, it can be seen that the dielectric functions corresponding to the functionals are different over the entire spectrum of the photon energy only for the MnPc, FePc, and CoPc. Why does the NiPc fall out of this row? The answer to this question is sought in Table 3. It turns out that the magnetic moment of the entire molecule NiPc is zero. Therefore, it becomes clear why dielectric functions for both values of the mixing coefficient are almost identical. From Fig. 4, we see that the dielectric functions of the NiPc and CoPc, corresponding to different values of the mixing factor, are close to each of these materials. For ZnPc, the dielectric functions, corresponding to different values of the mixing parameter, are identical throughout the spectrum of the photon energies under consideration. The dielectric constants depicted in Fig. 4 allow us to draw the following conclusions. Significant differences in the dielectric functions of the MnPc, FePc, and CoPc, corresponding to different mixing parameters, are due to the strong hybridization of the 3d states of the transition elements with the states in the valence and conduction bands. In the materials of NiPc and CuPc, this hybridization is less pronounced. For the CuPc material, it is even weaker.


1. F.A. Sarı, M. Kazici, E. Harputlu, S. Bozar, Koyun, Y. Sahin, N. Ugur, M. Ince, S. Günes. Zn phthalocyanine derivatives for solution-processed small molecule organic solar cells. *Chemistry Select* bf 3, 13692 (2018).
2. C.J. Lim, M.G. Park, M.S. Kim, J.H. Han, S. Cho, M.-H. Cho, Y. Yi, H. Lee, S.W. Cho. Electronic structure of $C_{60}$/zinc phthalocyanine/$V_2O_5$ interfaces studied using photoemission spectroscopy for organic photovoltaic applications. *Molecules* **23**, 449 (2018).
3. J. Benduhn, F. Piersimoni, G. Londi, A. Kirch, J. Widmer, C. Koerner, D. Beljonne, D. Neher, D. Spoltore, K. Vandewal. Impact of triplet excited states on the open-circuit voltage of organic solar cells. *Adv. Energy Mater.* **8**, 1800451 (2018).
4. J. Yu, Z. Jiang, Y. Hao, Q. Zhu, M. Zhao, X. Jiang, J. Zhao. Two dimensional self-assembly zinc porphyrin and zinc phthalocyanine heterojunctions with record high power conversion efficiencies. *J. Phys.: Condensed Matter.* **30**, 25LT02 (2018).
5. M.D. Pavlova, I.A. Lamkin, S.A. Tarasov, A.V. Solomonov. Organic photodetective device based on metal phthalocyanine. *J. Phys.: Conference Series* **1038**, 012104 (2018).
6. S. Ahmadi, M.N. Shariati, S. Yu, M. Göthelid. Molecular layers of ZnPc and FePc on Au(111) surface: Charge transfer and chemical interaction. *J. Chem. Phys.* **137**, 084705 (2012).

7. T. Lei, H. Dong, J. Xi, Y. Niu, J. Xu, F. Yuan, B. Jiao, W. Zhang, X. Hou, Z. Wu. Highly-efficient and low-temperature perovskite solar cells by employing a Bi-hole transport layer consisting of vanadium oxide and copper phthalocyanine. *Chem. Commun.* **54**, 6177 (2018).
8. Q. Hu, E. Rezaee, Q. Dong, H. Shan, Q. Chen, L. Wang, B. Liu, J.-H. Pan, Z.-X. Xu. P3HT/phthalocyanine nanocomposites as efficient hole-transporting materials for perovskite solar cells. *Solar RRL* **3**, 1800264 (2019).
9. C.A. Betty, N. Padma, S. Arora, P. Survaiya, D. Bhattacharya, S. Choudhury, M. Roy. Porous silicon-copper phthalocyanine heterostructure based photoelectrochemical cell. *Appl. Surface Sci.* **428**, 463 (2018).
10. H. Kim, H.G. Park, M.-J. Maeng, Y.R. Kang, K.R. Park, J. Choi, Y. Park, Y.D. Kim, C. Kim. Multifunctional bilayer template for near-infrared-sensitive organic solar cells. *ACS Applied Materials & Interfaces* **10**, 16681 (2018).
11. M.-S. Choi, S. Lee, H.J. Kim, J.-J. Kim. Inverted near-infrared organic photodetector with oriented lead (II) phthalocyanine molecules via substrate heating. *Organic Electronics* **61**, 164 (2018).
12. P. Brogdon, H. Cheema, J.H. Delcamp. Near-infrared-absorbing metal-free organic, porphyrin, and phthalocyanine sensitizers for panchromatic dye-sensitized solar cells. *Chem. Sus. Chem.* **11**, 86 (2018).
13. A. Sreedevi, K.P. Priyanka, K.K. Babitha, S.I. Sankararaman, V. Thomas. Synthesis and characterization of silver tungstate/iron phthalocyanine nanocomposite for electronic applications. *Europ. Phys. J. B* **90**, 102 (2017).
14. D. Zhao, H. Liu, Y. Miao, H. Wang, B. Zhao, Y. Hao, F. Zhu, B. Xu. A red tandem organic light-emitting diode based on organic photovoltaic-type charge generation layer. *Organic Electronics* **32**, 1 (2016).
15. S.A. Choi, K. Kim, S.J. Lee, H. Lee, A. Babajanyan, B. Friedman, K. Lee. Effects of thermal preparation on Copper Phthalocyanine organic light emitting diodes. *J. Lumines.* **171**, 149 (2016).
16. B. Ghazal, E.N. Kaya, A. Husain, A. Ganesan, M. Durmuş, S. Makhseed. Biotinylated-cationic zinc(II) phthalocyanine towards photodynamic therapy. *J. Porphyrins and Phthalocyanines* **23**, 46 (2019).
17. D.C. Soler, J. Ohtola, H. Sugiyama, M.E. Rodriguez, L. Han, N.L. Oleinick, M. Lam, E.D. Baron, K.D. Cooper, T.S. McCormick. Activated T cells exhibit increased uptake of silicon phthalocyanine Pc 4 and increased susceptibility to Pc 4-photodynamic therapy-mediated cell death. Photochem. *Photobiol. Sci.* **15**, 822 (2016).
18. A. Kvitschal, I. Cruz-Cruz, I.A. Hümmelgen. Copper phthalocyanine based vertical organic field effect transistor with naturally patterned tin intermediate grid electrode. *Organic Electronics* **27**, 155 (2015).
19. A. Rydosz, E. Maciak, K. Wincza, S. Gruszczynski. Microwave-based sensors with phthalocyanine films for acetone, ethanol and methanol detection. *Sensors and Actuators B: Chem.* **237**, 876 (2016).
20. H. Xu, C. Liao, Y. Liu, B.-C. Ye, B. Liu. Iron Ppthalocyanine decorated nitrogen-doped graphene biosensing platform for real-time detection of nitric oxide released from living cells. *Analytical Chem.* **90**, 4438 (2018).
21. T. Soganci, Y. Baygu, N. Kabay, Y. Gök, M. Ak. Comparative investigation of peripheral and nonperipheral zinc phthalocyanine-based polycarbazoles in terms of optical, electrical, and sensing properties. *ACS Appl. Mater. & Interfaces* **10**, 21654 (2018).
22. J. Hu, R. Wu. Control of the magnetism and magnetic anisotropy of a single-molecule magnet with an electric field. *Phys. Rev. Lett.* **110**, 097202 (2013).
23. T. Gredig, C.N. Colesniuc, S.A. Crooker, I.K. Schuller. Substrate-controlled ferromagnetism in iron phthalocyanine films due to one-dimensional iron chains. *Phys. Rev. B* **86**, 014409 (2012).
24. A. Candini, V. Bellini, D. Klar, V. Corradini, R. Biagi, V. De Renzi, K. Kummer, N.B. Brookes, U. del Pennino, H. Wende *et al.* Ferromagnetic exchange coupling between Fe phthalocyanine and Ni(111) surface mediated by the extended states of graphene. *J. Phys. Chem. C* **118**, 17670 (2014).
25. W. Kuch, M. Bernien. Controlling the magnetism of adsorbed metal–organic molecules. *J Phys.: Cond. Matter.* **29**, 023001 (2016).
26. I.E. Brumboiu, S. Haldar, J. Luder, O. Eriksson, H.C. Herper, B. Brena, B. Sanyal. Influence of electron correlation on the electronic structure and magnetism of transition-metal phthalocyanines. *J. Chem. Theory and Computation* **12**, 1772 (2016).
27. C. Adamo, G.E. Scuseria, V. Barone. Accurate excitation energies from time-dependent density functional theory: Assessing the PBE0 model. *J. Chem. Phys.* **111**, 2889 (1999).
28. C.A. Guido, E. Brémond, C. Adamo, P. Cortona. Communication: One third: A new recipe for the PBE0 paradigm. *J. Chem. Phys.* **138**, 021104 (2013).
29. J. Sun, R.C. Remsing, Y. Zhang, Z. Sun, A. Ruzsinszky, H. Peng, Z. Yang, A. Paul, U. Waghmare, X. Wu *et al.* Accurate first-principles structures and energies of diversely bonded systems from an efficient density functional. *Nature Chem.* **8**, 831 (2016).
30. J.P. Perdew, K. Burke, M. Ernzerhof. Generalized gradient approximation made simple. *Phys. Rev. Lett.* **77**, 3865 (1996).
31. P.E. Blöchl. Projector augmented-wave method. *Phys. Rev. B* **50**, 17953 (1994).
32. X. Gonze, F. Jollet, F. Abreu Araujo, D. Adams, B. Amadon, T. Applencourt, C. Audouze, J.-M. Beuken, J. Bieder, A. Bokhanchuk *et al.* Recent developments in the ABINIT software package. *Comp. Phys. Commun.* **205**, 106 (2016).
33. I.E. Brumboiu, S. Haldar, J. Lüder, O. Eriksson, H.C. Herper, B. Brena, B. Sanyal. Influence of electron correlation on the electronic structure and magnetism of transition-metal phthalocyanines. *J. Chem. Theory and Computation* **12**, 1772 (2016).

34. B.E. Williamson, T.C. VanCott, M.E. Boyle, G.C. Misener, M.J. Stillman, P.N. Schatz. Determination of the ground state of manganese phthalocyanine in an argon matrix using magnetic circular dichroism and absorption spectroscopy. *J. Amer. Chem. Soc.* **114**, 2412 (1992).
35. S. Heutz, C. Mitra, W. Wu, A. Fisher, A. Kerridge, M. Stoneham, A. Harker, J. Gardener, H.-H. Tseng, T. Jones *et al.* Molecular thin films: A new type of magnetic switch. *Adv. Materials* **19**, 3618 (2007).
36. T. Kroll, R. Kraus, R. Schönfelder, V.Y. Aristov, O.V. Molodtsova, P. Hoffmann, M. Knupfer. Transition metal phthalocyanines: Insight into the electronic structure from soft x-ray spectroscopy. *J. Chem. Phys.* **137**, 054306 (2012).
37. D. Stradi, C. Díaz, F. Martín, M. Alcamí. A density functional theory study of the manganese-phthalocyanine. *Theor. Chem. Accounts* **128**, 497 (2011).
38. M.-S. Liao, S. Scheiner. Electronic structure and bonding in metal phthalocyanines, Metal=Fe, Co, Ni, Cu, Zn, Mg. *J. Chem. Phys.* **114**, 9780 (2001).
39. P.S. Miedema, S. Stepanow, P. Gambardella, F.M.F. de Groot. 2p x-ray absorption of iron-phthalocyanine. *J. Phys.: Conf. Ser.* **190**, 012143 (2009).
40. M. Evangelisti, J. Bartolome, L.J. de Jongh, G. Filoti. Magnetic properties of $\alpha$-iron(II) phthalocyanine. *Phys. Rev. B* **66**, 144410 (2002).
41. S. Baba, A. Suzuki, T. Oku. Electronic structures and magnetic/ optical properties of metal phthalocyanine complexes. *AIP Conf. Proc.* **1709**, 020012 (2016).
42. N. Ishikawa. *Phthalocyanine-Based Magnets* (Springer, 2010) [ISBN: 978-3-642-04752-7].
43. S. Stepanow, P.S. Miedema, A. Mugarza, G. Ceballos, P. Moras, J.C. Cezar, C. Carbone, F.M.F. de Groot, P. Gambardella. Mixed-valence behavior and strong correlation effects of metal phthalocyanines adsorbed on metals. *Phys. Rev. B* **83**, 220401 (2011).
44. N. Marom, X. Ren, J.E. Moussa, J.R. Chelikowsky, L. Kronik. Electronic structure of copper phthalocyanine from $G_0W_0$ calculations. *Phys. Rev. B* **84**, 195143 (2011).
45. S.A. Fischer, C.J. Cramer, N. Govind. Excited-state absorption from real-time time-dependent density functional theory: Optical limiting in zinc phthalocyanine. *J. Phys. Chem. Lett.* **7**, 1387 (2016).
46. L. Meng, K. Wang, Y. Han, Y. Yao, P. Gao, C. Huang, W. Zhang, F. Xu. Synthesis, structure, and optical properties of manganese phthalocyanine thin films and nanostructures. *Progr. Natural Sci.: Mater. Intern.* **27**, 329 (2017).
47. R. Seoudi, G. El-Bahy, Z. E. Sayed. Ultraviolet and visible spectroscopic studies of phthalocyanine and its complexes thin films. *Opt. Mater.* **29**, 304 (2006).
48. M.M. El Nhass, H.S. Soliman, H.S. Metwally, A.M. Farid, A.A.M. Farag, A.A. El Shazly. Optical properties of evaporated iron phthalocyanine(FePc) thin films. *J. Optics* **30**, 121 (2001).
49. K.-J. Huang, Y.-S. Hsiao, W.-T. Whang. Selective growth and enhanced field emission properties of micropatterned iron phthalocyanine nanofiber arrays. *Organ. Electron.* **12**, 1826 (2011).
50. A. Gadalla, O. Crégut, M. Gallart, B. Hönerlage, J.-B. Beaufrand, M. Bowen, S. Boukari, E. Beaurepaire, P. Gilliot. Ultrafast optical dynamics of metal-free and cobalt phthalocyanine thin films. *J. Phys. Chem. C* **114**, 4086 (2010).
51. M.M. EL-NAHASS, K.F. Abd-El-Rahman, A.A.M. Farag, A.A.A. Darwish. Optical characterisation of thermally evaporated nickel phthalocyanine thin films. *Intern. J. Mod. Phys. B* **18**, 421 (2004).
52. M. Sayyad, M. Shah, K. Karimov, Z. Ahmad, M. Saleem, M.M. Tahir. Fabrication and study of NiPc thin film based surface type photocapacitors. *J. Optoelectron. Adv. Mater.* **10**, 2805 (2008).
53. A. Djurišić, C. Kwong, T. Lau, W. Guo, E. Li, Z. Liu, H. Kwok, L. Lam, W. Chan. Optical properties of copper phthalocyanine. *Optics Commun.* **205**, 155 (2002).
54. Z.T. Liu, H.S. Kwok, A.B. Djurišić. The optical functions of metal phthalocyanines. *J. Phys. D: Appl. Phys.* **37**, 678 (2004).
55. S. Senthilarasu, S. Velumani, R. Sathyamoorthy, A. Subbarayan, J. Ascencio, G. Canizal, P. Sebastian, J. Chavez, R. Perez. Characterization of zinc phthalocyanine (ZnPc) for photovoltaic applications. *Appl. Phys. A* **77**, 383 (2003).


Received 14.08.19

*Ю.В. Клиско, С.В. Сиротюк*

ДОСЛІДЖЕННЯ ЕЛЕКТРОННИХ ВЛАСТИВОСТЕЙ МЕТАЛО-ФТАЛОЦІАНІНІВ ЗА ДОПОМОГОЮ ГІБРИДНОГО ФУНКЦІОНАЛА

В даній роботі представлено дослідження метало-фталоціанінів з використанням гібридного функціонала. Досліджені фталоціаніни містили атоми перехідних металів, а саме марганець, залізо, кобальт, нікель, мідь та цинк. Проведено розрахунок ізольованих молекул. Для фталоціаніну з атомом заліза було проведено розрахунки з чотирма параметрами змішування: 0, 1/4, 1/3 та 1/2. Для всіх інших молекул ми провели розрахунки з двома значеннями: 1/4 та 1/3. В роботі наведено основні параметри електронної структури, такі як енергетична щілина між заселеними та незаселеними рівнями, намагніченість, а також графіки залежності уявної частини діелектричної функції від енергії фотона в порівнянні з експериментальними спектрами поглинання. Фталоціаніни із марганцем, залізом та кобальтом мають сильну залежність електронних властивостей від величини доданої точної обмінної взаємодії. Тоді як в молекулах з нікелем, міддю та цинком зміна цієї величини суттєво не впливає на отримані результати.

*Ключові слова:* металоорганічні матеріали, гібридний функціонал.